Coherent Association of Single Molecules from Single Atoms

A DISSERTATION PRESENTED
BY
YICHAO YU
TO
THE DEPARTMENT OF PHYSICS

IN PARTIAL FULFILLMENT OF THE REQUIREMENTS
FOR THE DEGREE OF
DOCTOR OF PHILOSOPHY
IN THE SUBJECT OF
PHYSICS

HARVARD UNIVERSITY
CAMBRIDGE, MASSACHUSETTS
MARCH 2021

Thesis advisor: Professor Kang-Kuen Ni   Yichao Yu

Coherent Association of Single Molecules from Single Atoms

ABSTRACT

Contents

Acknowledgments

,

0
Introduction

1

Apparatus

1.1 Cooling and Optical Pumping Beams

(MOT, OP, fiber back reflection)

(Mention Na Raman beam to be covered in later chapter?)

1.2 Tweezer and Imaging

1.3 Molecular Raman Frequency Generation

(beam path, calibration)

2

Computer Control of the Experiment

2.1 Overall Structure

2.2 Frontend

(Abstraction) (Backward compatibility) (Flexibility) (Text based/version control friendly)

2.3 Backends

(communication protocol) (IR)

2.3.1 FPGA Backend

(clock generation) (pulse merging) (compression)

2.3.2 NiDAQ Backend

(Variable clock)

2.3.3 USRP Backend

(SIMD)

2.4 Automation of Scan

(Scan requirement) (Combination of scans) (Scope/nested structure)

2.5 Summary and Outlook

(new backend/SPCM) (native code generation, auto vectorization) (dynamic logic and dependency tracking/optimization)

3

Raman Sideband Cooling

3.1 Introduction

(In order to achieve full quantum control on molecules, we need to control atoms first.) (An example of such control) (Motional degrees of freedom) (PGC cools to ...) (RSC to further cool.)

Figure 3.1: Single Na atom Raman sideband cooling scheme. The Raman transitions couples $|2, 2; n\rangle$ and $|1, 1; n + \Delta n\rangle$ through the intermediate states $|e_i\rangle$ in the $3^2 P_{3/2}$ electronic states. The transitions have a one-photon detuning $\Delta_i \approx 75$ GHz. Two-photon detuning, δ, is defined relative to the $\Delta n = 0$ carrier transition. For optical pumping, we use two σ^+ polarized transitions, one to pump the atom state out of $|1, 1\rangle$ via $3^2 P_{3/2}$ and one to pump atoms out of $|2, 1\rangle$ via $3^2 P_{1/2}$ to minimize heating of the $|2, 2\rangle$ state.

3.2   Basic Theory

The relevant energy diagram and the laser frequencies for RSC are shown in Fig. 3.1. We approximate the trapping potential using a harmonic oscillator. Since this is a separable potential, we can use only the 1D motional state $|n\rangle$ and the result can be easily generalized to the full 3D system.

The cooling sequence consists of two types of pulses. First, a Raman pulse drives the atom to a different hyperfine state while simultaneously reduces the motional energy of the atom. The optical pumping (OP) pulse afterwards then reset the hyperfine state of the atom and reduce the entropy of the system. In this section, we will discuss the theory of each types of pulses individually. We will cover how the pulses affect cooling performance in section 3.5.

3.2.1   Raman Transition

As shown in Fig. 3.1, the cooling sequence starts with the sodium atom in the $|s_1\rangle \equiv |2, 2\rangle$ hyperfine state, and a Raman transition is used to drive the atom to the $|s_2\rangle \equiv |1, 1\rangle$ state, where $|F, m_F\rangle$ denotes the F and m_F quantum number for the sodium atom. The full Rabi frequency for such a transition is given by

$$\Omega_R^0 = \sum_i \frac{\Omega_{1i}\Omega_{2i}^*}{2\Delta_i}$$

where the sum is over all the coupled excited states, $\Omega_{ai} \equiv \langle a|\mathbf{d} \cdot \mathbf{E}_a|e_i\rangle$ is the single photon Rabi frequency between $|a\rangle$ and $|e_i\rangle$ and Δ_i is the single photon detuning from excited state $|e_i\rangle$.

8

In order to account for the motional degrees of freedom, we need to include the spatial wavefunction of the atom and light into account. As mentioned above, we approximate the atomic motional wavefunction by the harmonic oscillator eigenstates $|n\rangle$. Coupling between states different n states from the Raman transition is allowed due to the recoil from the Raman lasers, which corresponds to a spacial phase imprinting of $e^{i\mathbf{\Delta k}\cdot\hat{\mathbf{x}}}$ where $\mathbf{\Delta k}$ is the wavevector difference between the two Raman beams. Using the creation ($\hat{a}^\dagger$) and annihilation ($\hat{a}$) operators and the relation $\hat{\mathbf{x}} = \mathbf{x}_0(\hat{a}+\hat{a}^\dagger)$ where $x_0 = \sqrt{\hbar/2m\omega}$ is the harmonic oscillator length, the phase factor can be expressed as $e^{i\eta_R(\hat{a}+\hat{a}^\dagger)}$ where $\eta_R \equiv \mathbf{\Delta k} \cdot \mathbf{x}_0$ is the Lamb-Dicke parameter for the Raman transition . The matrix element between motional state $|n\rangle$ and $|n'\rangle$ is therefore,

$$M_{n,n'} = \langle n|e^{i\eta_R(\hat{a}+\hat{a}^\dagger)}|n'\rangle$$

and the final Raman Rabi frequency between motional states n and n' is given by,

$$\Omega_R^{n,n'} = M_{n,n'}\Omega_R^0$$

For $n = n'$, this is called a carrier transition and the others are called sideband transitions. If the final state is higher than the initial one, i.e. $n' > n$, it is a heating sideband. Likewise, transitions with $n' < n$ are cooling sidebands.

A closed form result for $M_{n,n'}$ is given in ,

$$M_{n,n'} = e^{\eta_R^2/2} \sqrt{\frac{n_<!}{n_>!}} \eta_R^{|n-n'|} L_{n_<}^{|n-n'|}(\eta_R^2)$$

where $n_<$ and $n_>$ are the lesser and greater, respectively, of n and n', and L_n^α is the generalized Laguerre polynomial,

$$L_n^\alpha(x) \equiv \sum_{m=0}^{n} (-1)^m \begin{pmatrix} n + \alpha \\ n - m \end{pmatrix} \frac{x^m}{m!}$$

An important limit is the so-called Lamb-Dicke regime defined by $\eta_R^2(2n+1) \ll 1$. In this case, we can approximate the phase factor in leading order of η_R,

$$e^{i\eta_R(\hat{a}+\hat{a}^\dagger)} \approx 1 + i\eta_R(\hat{a} + \hat{a}^\dagger)$$

and the matrix element

$$M_{n,n'} \approx \delta_{n,n'} + i\eta_R \sqrt{n+1}\delta_{n+1,n'} + i\eta_R \sqrt{n}\delta_{n,n'+1}$$

the three terms corresponds to the carrier ($n' = n$), the first order heating sideband ($n' = n+1$) and the first order cooling sideband ($n' = n - 1$) with corresponding strength 1, $\eta_R\sqrt{n+1}$ and $\eta_R\sqrt{n}$. We can clearly see from this approximation that the coupling to other motional state is stronger for a larger η_R and higher motional quantum number n. We will discuss this effect outside the Lamb-Dicke regime and its implication on the cooling performance in more detail in section 3.5.

3.2.2 Optical Pumping

Driving the system on a cooling sideband with Raman transition can reduce the motional energy of the atom. However, this is a fully coherent process that does not reduce the system entropy and is not really "cooling" the system or achieving better control on the quantum state of the system. Instead, quantum state control is achieved in the RSC via the OP pulse. The initial hyperfine state $|2, 2\rangle$ is a stretched state so it is the state the system naturally ends up in when σ^+ light is applied. However, if this is done using scattering from a $F = 2$ to $F' = 3$ transition, the OP beam will allow continuous photon cycle between the $|2, 2\rangle$ and the $|3', 3\rangle$ causing unnecessary motional heating during OP. Therefore, the OP must be done on a $F = 2$ to $F' = 2$ transition. Unfortunately, for Na, the corresponding transition from $3^2 S_{1/2}$ to $3^2 P_{3/2}$ that is used for the MOT is not useable due to the small energy difference of 60MHz (or 6 line widths) between the $F' = 2$ and $F' = 3$ states[Steck]. Instead, we must use the sodium D1 line, i.e. $3^2 S_{1/2}$ to $3^2 P_{1/2}$ transition, which lacks a $F' = 3$ excited state. The D1 light with σ^+ polarization is only used to pump atoms from $F = 2$ states (in particular $|2, 1\rangle$ which is populated during the OP process). Since the goal of the OP pulse is to clear the atom population in all states but $|2, 2\rangle$, the photon cycling is not a concern for $F = 1$ states and the D2 line is used for OP of $F = 1$ states instead. This also allow us to reuse the MOT light source and simplifies our setup.

3.3 Raman Sideband Thermometry

From the discussion in section 3.2.1, we see that the strength of the sideband transition depends on the initial motional state as well as the Lamb-Dicke parameter η_R of the atom. This dependency allows us to infer the motional state of the atom by measuring the sideband height, i.e. the so-called sideband thermometry.

In particular, for atom with temperature T, the probability for the atom to be in motional state $|n\rangle$ is,

$$p_n = \frac{\mathrm{e}^{-n\hbar\omega/k_B T}}{1 - \mathrm{e}^{-\hbar\omega/k_B T}}$$

for a Raman pulse with full Rabi frequency Ω_R^0 and time t, the peak height for the first order heating (+) and cooling (-) sidebands,

$$b_\pm = \sum_{n=0}^{\infty} p_n \sin^2\left(\frac{\Omega_R^0 t}{2} M_{n,n\pm1}\right)$$

note that $p_{n+1} = p_n \mathrm{e}^{-\hbar\omega/k_B T}$, $M_{n,n'} = M_{n',n}$ and $M_{n,-1} = 0$, we have

$$b_- = \sum_{n=0}^{\infty} p_n \sin^2\left(\frac{\Omega_R^0 t}{2} M_{n,n-1}\right)$$

$$= \mathrm{e}^{-\hbar\omega/k_B T} \sum_{n=1}^{\infty} p_{n-1} \sin^2\left(\frac{\Omega_R^0 t}{2} M_{n-1,n}\right)$$

$$= \mathrm{e}^{-\hbar\omega/k_B T} b_+$$

Therefore, if we measure the ratio of the cooling and heating sideband heights $\alpha \equiv h_-/h_+$, we can calculate the temperature of the atom with $e^{-\hbar\omega/k_B T} = \alpha$. The corresponding ground state probability is,

$$p_0 = \frac{1}{1 - e^{-\hbar\omega/k_B T}}$$
$$= \frac{1}{1 - \alpha}$$

We will use this to experimentally characterize the performance of the cooling sequence in the following sections.

3.4 Setup

The geometry of all the beams and field involved is shown in Fig. 3.2. In order to make the cooling more efficient and simplify the sideband thermometry, we address the motion along the three principle axis of the tweezer using different pairs of Raman beams. We apply an external bias magnetic field of 8.8G parallel to the polarization of the tweezer beam (and orthogonal to the tweezer beam propagation direction). This makes the field orthogonal to the effective magnetic field of the tweezer, which minimizes the vector light shifts [Kaufman et al.,Thompson et al.]. Since the optical pumping beam requires σ^+ polarization, it is setup to propagate parallel to the applied magnetic field.

3.5 Cooling Performance and Challenge with Large Lamb-Dicke Parameter

3.3
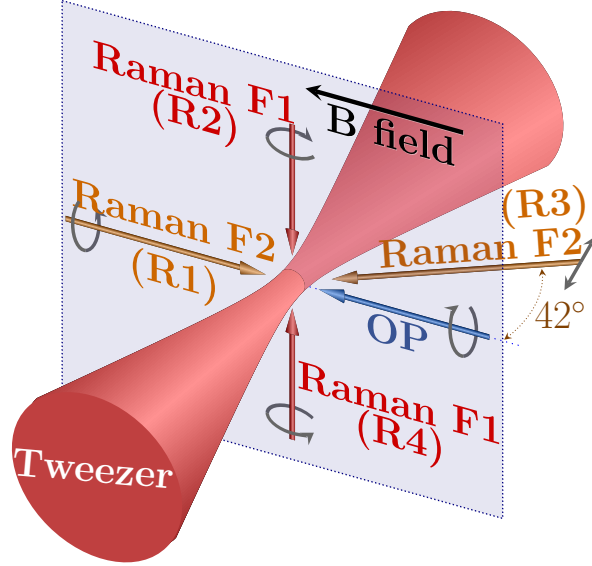
Figure 3.2: Geometry and polarizations of the Raman and optical pumping beams relative to the optical tweezer and bias magnetic field. Raman beams R1 and R4 address the radial x-mode. R1 and R2 address the radial y-mode. R3 and R4 address the axial z-mode, where the beams also couple to radial motion, but this coupling can be neglected when the atoms is cooled to the ground state of motion.
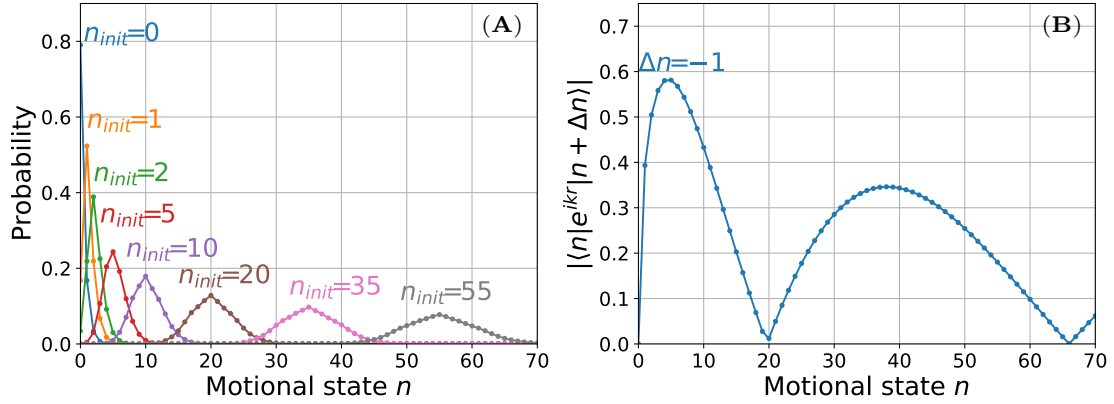
Figure 3.3: Optical pumping motional-state redistribution and Raman coupling for large LD parameters for the axial direction (z). The range plotted covers 95% of the initial thermal distribution. (A) Motional state distribution after one OP cycle for different initial states motion, n_{init}. Due to photon-recoil and the large LD parameter, $\eta_z^{\text{OP}} = 0.55$, there is a high probability of n changing. (B) Matrix elements for Raman transition on the first order cooling sideband deviate from $\sqrt{n}$ scaling with multiple minima.
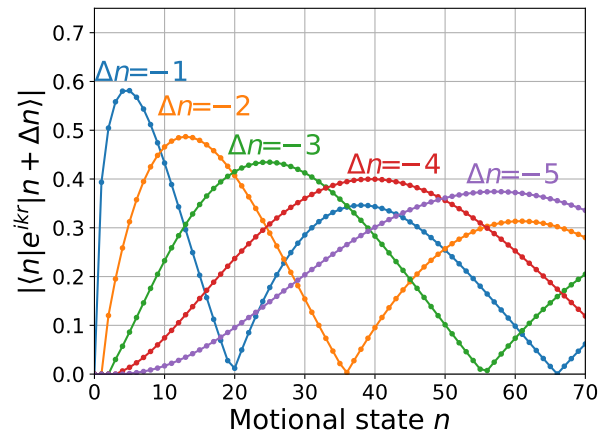
Figure 3.4: Matrix elements for Raman transition including high order sidebands. During cooling, we utilize the fact that high motional states couple most effectively to sidebands with large $|\Delta n|$ in order to overcome the issue with variation and dead zone in the coupling strengths.

3.6 Solution: High Order Sidebands

3.4

3.7 Solution: Simulation Based Optimization

3.5

3.8 Calibration

(Sideband/carrier) (Cold vs hot)

3.9 Cooling Performance

3.6 3.7
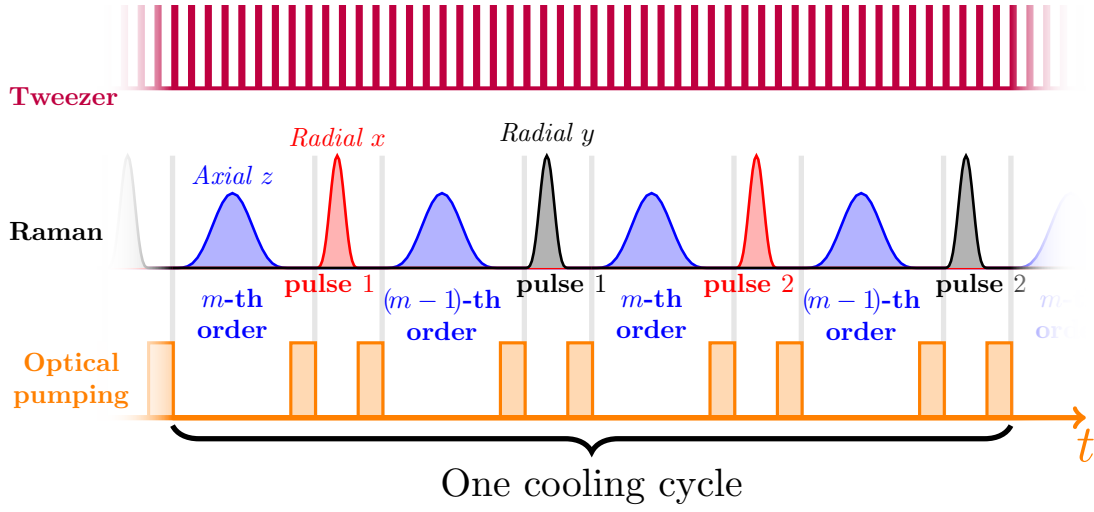
Figure 3.5: Schematic of the cooling pulse sequence. The tweezer is strobed at 3 MHz to reduce light shifts during optical pumping [Hutzler et al.]. Each cooling cycle consists of 8 sideband pulses. The four axial pulses address two sideband orders. The two pulses in each radial direction either address $\Delta n = -2$ and $\Delta n = -1$ or have different durations to drive $\Delta n = -1$, at the end of the cooling sequence when most of the population is below $n = 3$. The Raman cooling and spectroscopy pulses have Blackman envelopes [Kasevich & Chu] to reduce off-resonant coupling, while the measurement Rabi pulses in Fig. 3.7 have square envelopes to simplify analysis.
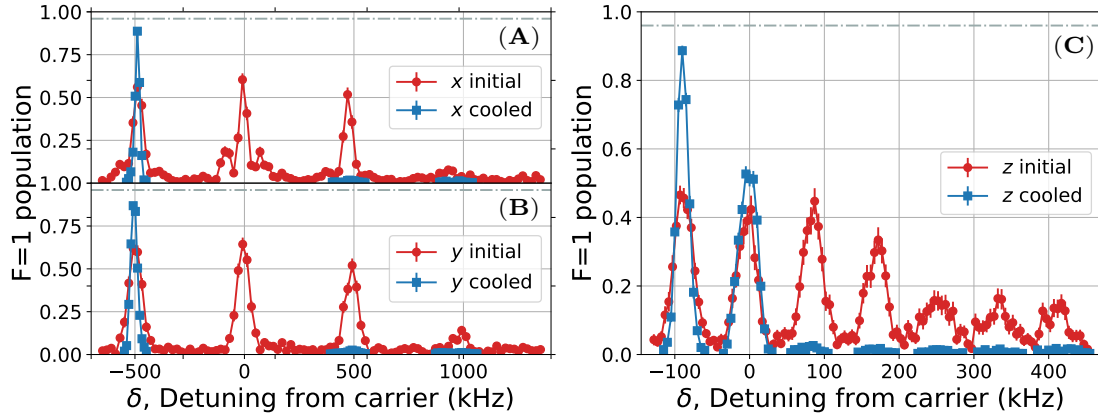
Figure 3.6: Raman sideband spectra for (A) x, (B) y, (C) z axis before (red circle) and after (blue square) applying Raman sideband cooling sequence. The height of the cooling sidebands (positive detuning) are strongly suppressed after cooling which suggests most of the atoms are cooled to the motional ground state in the trap.

Figure 3.7 (*following page*): Rabi flopping on radial axis x (A) carrier and (B) $\Delta n_x = 1$ sideband, radial axis y (C) carrier and (D) $\Delta n_x = 1$ sideband, axial axis z (E) carrier and (F) $\Delta n_x = 1$ sideband, before (red circle) and after (blue square) Raman sideband cooling.

Solid lines (both red and blue) in all plots are fits to a Rabi-flopping that includes a thermal distribution of motional states [Meekhof et al.] as well as off-resonant scattering from the Raman beams.

The blue lines correspond to a ground state probability of (A-D) 98.1% along radial axis and (E-F) 95% along the axial axis after cooling. The red lines correspond to a thermal distribution of $80\,\mu$K before RSC. The horizontal dashed lines in all the plots correspond to the $4\,\%$ probability of imaging loss.

The green dashed line in (F) includes the additional decoherence due to a fluctuation of the hyperfine splitting of magnitude 3 kHz. We see that the decoherence effect is strongest for the post-cooling data on the axial $\Delta n_z = 1$ sideband where the Rabi frequency is the lowest.
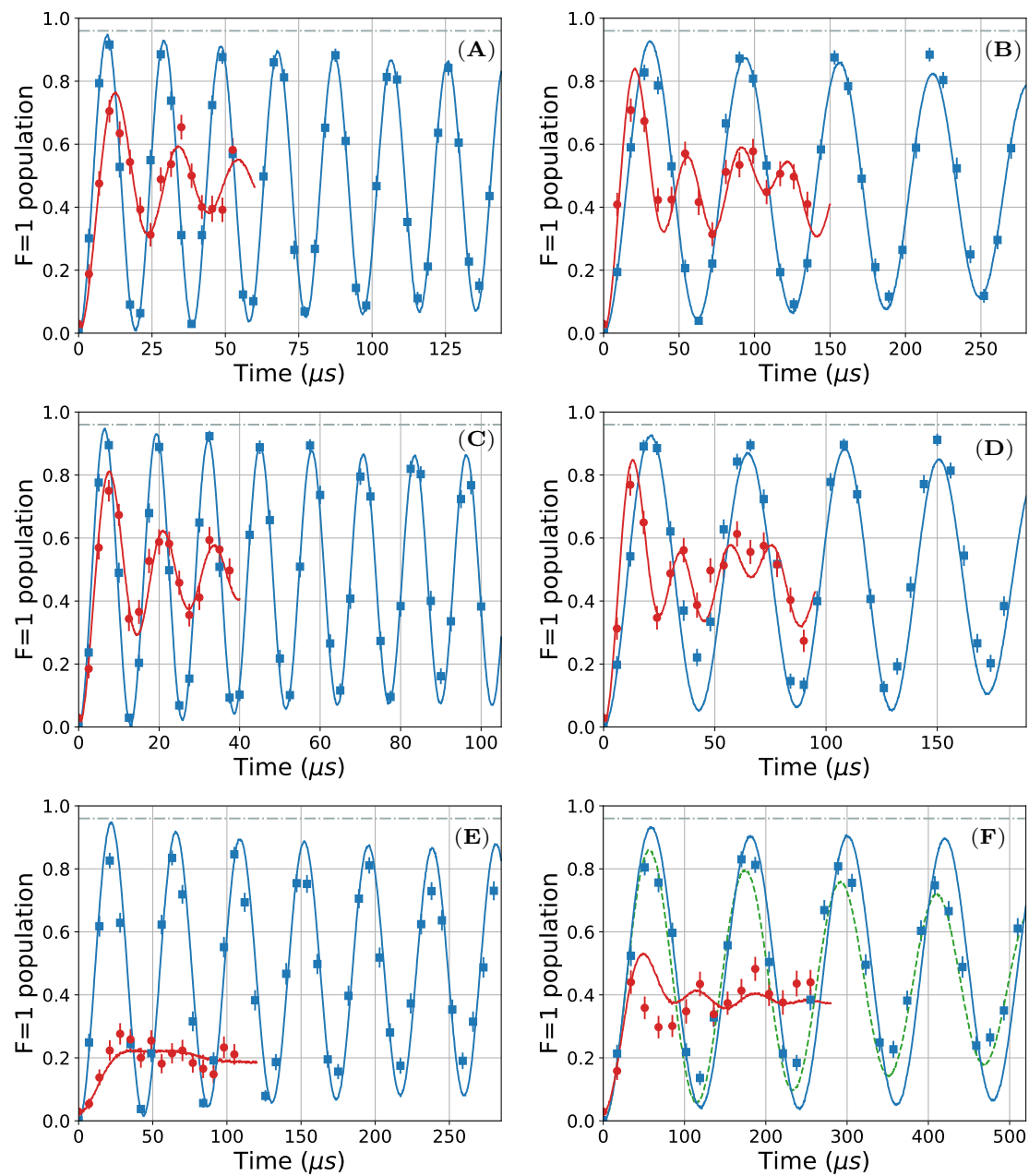
4

Interaction of Single Atoms

4.1 Scattering Length

(Importance/relation with binding energy etc.)

4.2 Energy Levels of Two Interacting Atoms in an Anisotropic Trap

(appendex?)

4.3 Interaction Shift Spectroscopy

(motional sideband, scattering length result)

4.4 Summary and Outlook

(Motional state selection)

5

Photoassociation of Single Atoms

(light shift, broadening)

5.3 Photoassociation Spectroscopy

(v=0, 12, 14, etc)

6

Two-photon Spectroscopy of NaCs

Ground State

7

Coherent Optical Creation of NaCs Molecule

7.1 Introduction

7.2 Raman Transition Beyond Three-Level Model

In an ideal three-level system, the scattering probability during a π pulse Raman transition can be made arbitrarily small by using a large single photon detuning. However, in a real system, there are often other effects that increases the scattering and may also put a lower limit on the scattering probability during the transfer. Fig. 7.1 shows a generic model for a real Raman transition demostrating some of these effects. Additionally, other practical limitation in the system like stability of the laser power and frequency also needs to be taken into account.

In the experiment, we find the parameter range that gives the best transfer efficiency using numerical simulation (see section 7.4). Nevertheless, in order to develop a general approach that can be applied to other systems, it is also important to understand the various physical mechanism that leads to the optimal parameters. Therefore, in this section, we will discuss some of the most important effects on the transfer efficiency at qualitative and semiquantitative level. Due to experimental

26

Figure 7.1: Generic model for a real Raman transition. The initial state $|i\rangle$ and the final state $|f\rangle$ has a energy difference δ and are coupled by two Raman beams with frequencies and single photon Rabi frequencies of ν_1, Ω_1 and ν_2, Ω_2 respectively. The corresponding matrix elements (arbitrary unit) are M_1 and M_2. The Raman beams are detuned by Δ from the primary excited state $|e\rangle$, which has a decay rate of Γ_e. We also consider additional states near the initial ($|i'\rangle$), final ($|f'\rangle$) and intermediate excited $|e'\rangle$ states which are separated from the corresponding Raman transition states by ω_i', ω_f' and ω_e' respectively. Only one additional state of each kinds are included to simplify the discussion without loss of generality.

constraint, we will assume that the single photon detuning is much smaller than the frequency of

each individual beams, i.e. $\Delta \ll \nu_1, \nu_2$.

7.2.1   ADDITIONAL INITIAL AND FINAL STATES

First, we will discuss the effect of $|i'\rangle$ and $|f'\rangle$ states near the initial and final states. These states can

be coupled to the excited state $|e\rangle$ by the Raman beams, which can in tern be coupled to the initial

and final states by an off-resonance Raman transition. The leakage is suppressed by the detuning from the Raman resonance, i.e. ω'_i and ω'_f. This puts a limit on the Raman Rabi frequency Ω_R to be smaller than the smallest energy gap, which in turns puts a limit on the minimum Raman transfer time. In our experiment, the minimum energy gap comes from axial motional excitation of the atomic initial states which is between $2\pi \times 10 - 30$ kHz depending on the trap depth used. The typical Raman π time we can realize is $0.5 - 5$ ms so this effect is not a major limiting factor for our transfer efficiency.

7.2.2   Additional Excited states

Next, we will consider the effect of the $|e'\rangle$ state near the excited intermediate state. These states can be coupled to the ground states, both $|i\rangle$ and $|f\rangle$, by the Raman beams and can cause a change in both the Raman Rabi frequency and the scattering rate. The total Raman Rabi frequency (Fig. 7.2A) is,

$$\Omega_{Raman} = \frac{\Omega_1 \Omega_2}{2\Delta} + \frac{\Omega'_1 \Omega'_2}{2(\Delta - \omega'_e)}$$

where Ω'_1 and Ω'_2 are the single photon Rabi frequencies coupling $|e'\rangle$ to $|i\rangle$ and $|f\rangle$ respectively. Depending on whether $\Omega'_1 \Omega'_2$ has the same (orange line) or different (blue line) sign as $\Omega_1 \Omega_2$, the total Raman Rabi frequency may be cancelled or enhanced between the two excited states. On the other hand, the total scattering rate (Fig. 7.2B) is almost always increased due to the additional state, creating a local minimum between the excited states. Combining the two effects, the ratio between the Raman Rabi frequency and the scattering rate, which determines the transfer efficiency, always
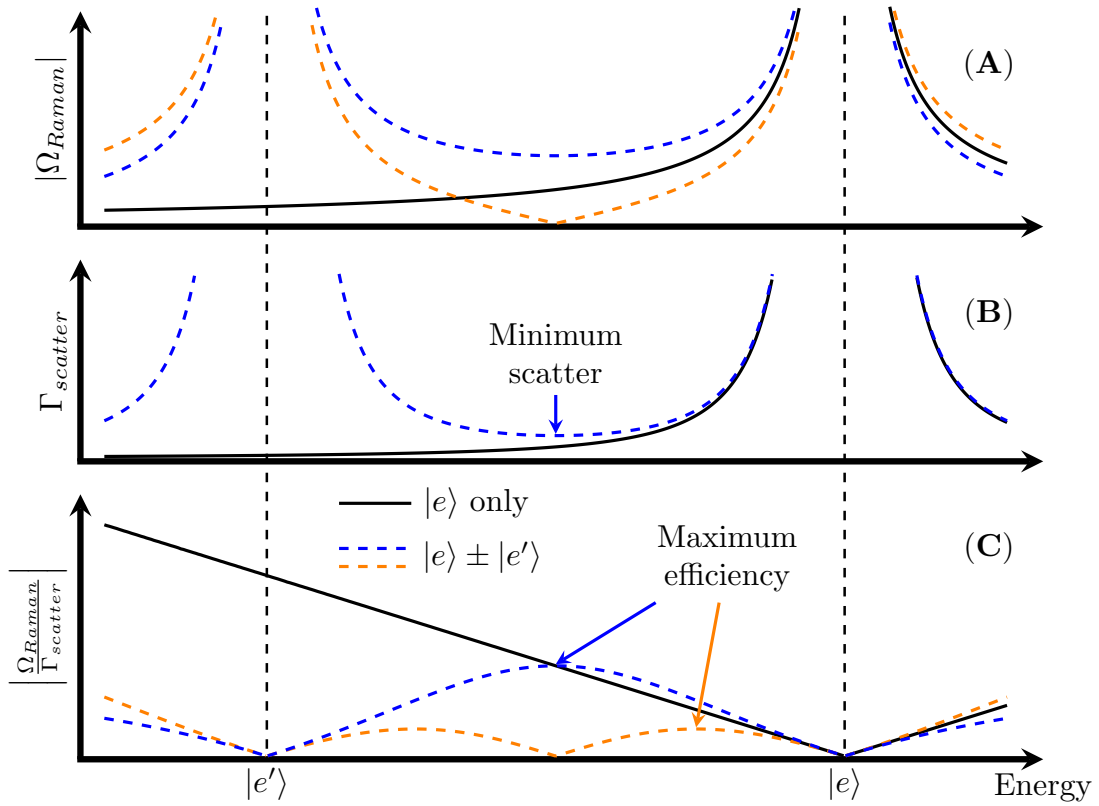
Figure 7.2: Effect of additional excited states $|e'\rangle$ on the Raman transition efficiency. (A) Depending on the sign of the coupling, there could be constructive (blue) or destructive (orange) interference on the Raman Rabi frequency Ω_{Raman}. (B) Increased scattering rate $\Gamma_{scatter}$ caused by $|e'\rangle$ with a minimal between the two states. (C) Optimal detunine exists between the two states with maximum transfer efficiency corresponds to a fraction of the state spacing.

have local maximum between the excited states (Fig. 7.2C).

Despite the difference in the position and value of the maximum for different $|e'\rangle$ parameters, we can summarize the effect on the transfer efficiency as a limit on the maximum detuning Δ_{max} to a fraction of the spacing between the excited states (ω'_e). As an example, the blue and orange maxima in Fig. 7.2C corresponds to a limit on single photon detuning of $0.5\omega'_e$ and $0.15\omega'_e$. As one would expected, a larger excited state spacing usually result in a larger detuning limit and a better transfer efficiency.

Summarizing the effect of additional excited state as a single number Δ_{max} allows us to keep using the equation for Raman transition with minor corrections and makes it easier to compare different state selection and transition schemes. It is also worth noting that although only one additional excited state $|e'\rangle$ is considered here, this result can be generalized when more excited states are taken into account as well. These states introduces additional smooth variation in both the Raman Rabi frequency and scattering rate and the effects on the final transition efficiency can be similarly treated as a change in the maximum detuning.

7.2.3 Cross Coupling Between Light Addressing Initial and Final States

Due to the small energy separation between the initial and final state δ, the cross coupling of the laser addressing the initial/final state on the final/initial state is another important effect in our experiment. Without the cross coupling, the total off resonance scattering rate for the initial and the final states is

$$\Gamma_{scatter0} = \frac{\Gamma_e \left(\Omega_1^2 + \Omega_2^2\right)}{4\Delta^2}$$

For a given Raman Rabi frequency $\Omega_{Raman} \propto \Omega_1 \Omega_2$, this is minimized when $\Omega_1 = \Omega_2$.

When cross coupling is taken into account, however, the total scattering rate becomes, [*]

$$\Gamma_{scatter} = \frac{\Gamma_e \Omega_1^2}{4M_1^2} \left(\frac{M_1^2}{\Delta^2} + \frac{M_2^2}{(\Delta + \delta)^2} \right) + \frac{\Gamma_e \Omega_2^2}{4M_2^2} \left(\frac{M_2^2}{\Delta^2} + \frac{M_1^2}{(\Delta - \delta)^2} \right) \tag{7.1}$$

$$\propto \frac{\Gamma_e P_1}{4} \left(\frac{M_1^2}{\Delta^2} + \frac{M_2^2}{(\Delta + \delta)^2} \right) + \frac{\Gamma_e P_2}{4} \left(\frac{M_2^2}{\Delta^2} + \frac{M_1^2}{(\Delta - \delta)^2} \right) \tag{7.2}$$

where $P_{1,2} \propto \Omega_{1,2}^2 / M_{1,2}^2$ are the powers of the laser beams 1 and 2. When $\delta \ll \Delta$ such as our experiment,

$$\Gamma_{scatter} \approx \frac{\Gamma_e \left(M_1^2 + M_2^2 \right)}{4\Delta^2} \left(\frac{\Omega_1^2}{M_1^2} + \frac{\Omega_2^2}{M_2^2} \right)$$

$$\propto \frac{\Gamma_e \left(M_1^2 + M_2^2 \right)}{4\Delta^2} (P_1 + P_2)$$

For a given Raman Rabi frequency $\Omega_{Raman} \propto \Omega_1 \Omega_2 \propto \sqrt{P_1 P_2}$, this is minimized when $P_1 = P_2$. Hence, due to the strong cross coupling, we need to use the same power in both Raman beams rather than adjusting the powers to match their single photon Rabi frequencies.

Moreover, at the minimum scattering rate, we have $\Omega_2 = \Omega_1 M_2 / M_1$ and the ratio between

---

[*]Here we assume that the matrix elements are the same for the two beams. This is the case when the two beams have the same polarization as in our experiment. This effect can be minimized or eliminated by selecting different polarizations for the two laser frequencies that does not couple to the other initial/final state. This would also require choosing an excited state with the same or lower angular momentum as the ground states in order to avoid cross coupling to different excited states.

Raman Rabi frequency and scattering rate is,

$$
\begin{aligned}
\frac{\Omega_{Raman}}{\Gamma_{scatter}} &= \frac{\Omega_1\Omega_2}{2\Delta} \frac{4\Delta^2}{\Gamma_e\left(M_1^2 + M_2^2\right)} \bigg/ \left(\frac{\Omega_1^2}{M_1^2} + \frac{\Omega_2^2}{M_2^2}\right) \\
&= \frac{2\Delta\Omega_1\Omega_2}{\Gamma_e\left(M_1^2 + M_2^2\right)} \bigg/ \left(\frac{\Omega_1^2}{M_1^2} + \frac{\Omega_2^2}{M_2^2}\right) \\
&= \frac{\Delta\Omega_1^2 M_2}{\Gamma_e M_1\left(M_1^2 + M_2^2\right)} \frac{M_1^2}{\Omega_1^2} \\
&= \frac{\Delta}{\Gamma_e} \frac{M_1 M_2}{M_1^2 + M_2^2}
\end{aligned}
$$

Therefore, for a given excited state linewidth Γ_e and maximum detuning (section 7.2.2) the transfer efficiency maximizes for the smallest $M_1 M_2/(M_1^2 + M_2^2)$ which happens when the ratio M_1/M_2 is the closest to 1.

The light shift of the Raman resonance is similarly affected by the cross coupling. The differential light shift between the initial and the final state determines the resonance fluctuation as a function of light intensity fluctuation. The ration between the light shift and the Raman Rabi frequency, i.e. line width, determines the stability requirement of our laser indensity. With cross coupling, the differential shift is (assuming $\delta \ll \Delta$),

$$
\begin{aligned}
\Delta\delta &\approx \frac{\Omega_1^2}{4\Delta} - \frac{\Omega_1^2 M_2^2}{4\Delta M_1^2} - \frac{\Omega_2^2}{4\Delta} + \frac{\Omega_2^2 M_1^2}{4\Delta M_2^2} \\
&= \frac{M_1^2 - M_2^2}{4\Delta}\left(\frac{\Omega_1^2}{M_1^2} + \frac{\Omega_2^2}{M_2^2}\right) \\
&\propto \frac{M_1^2 - M_2^2}{4\Delta}\left(P_1 + P_2\right)
\end{aligned}
$$

which is also minimized when $P_1 = P_2$ at a given Raman Rabi frequency.

The ratio with the Raman Rabi frequency is,

$$\frac{\Delta\delta}{\Omega_{Raman}} \approx \frac{M_1^2 - M_2^2}{4\Delta}\left(\frac{\Omega_1^2}{M_1^2} + \frac{\Omega_2^2}{M_2^2}\right)\frac{2\Delta}{\Omega_1\Omega_2}$$
$$= \frac{M_1^2 - M_2^2}{2\Omega_1\Omega_2}\left(\frac{\Omega_1^2}{M_1^2} + \frac{\Omega_2^2}{M_2^2}\right)$$
$$= \frac{M_1^2 - M_2^2}{M_1 M_2}$$

the absolute value of which is also minimized when the ratio M_1/M_2 is the closest to 1.

Due to the coupling strength difference, we have $M_2 \gg M_1$ in our experiment, which means,

$$\left|\frac{\Delta\delta}{\Omega_{Raman}}\right| \approx \frac{M_2}{M_1}$$

In order to keep the resonance stable within the linewidth of the Raman resonance, i.e. Ω_{Raman}, we need to maintain a relative stability of $\Delta\delta$, therefore relative stability of the laser power to better than M_1/M_2.

7.3   RAMAN TRANSFER VERSUS STIRAP

An alternative method often used to create and prepare the internal states of ultracold molecule is stimulated Raman adiabatic passage (STIRAP). Compared to Raman transition, which uses detuning from the excited state to reduce scattering during the transfer, STIRAP relies on a superposition between the initial and final state as a dark state to achieve the same goal. The dark state in STIRAP
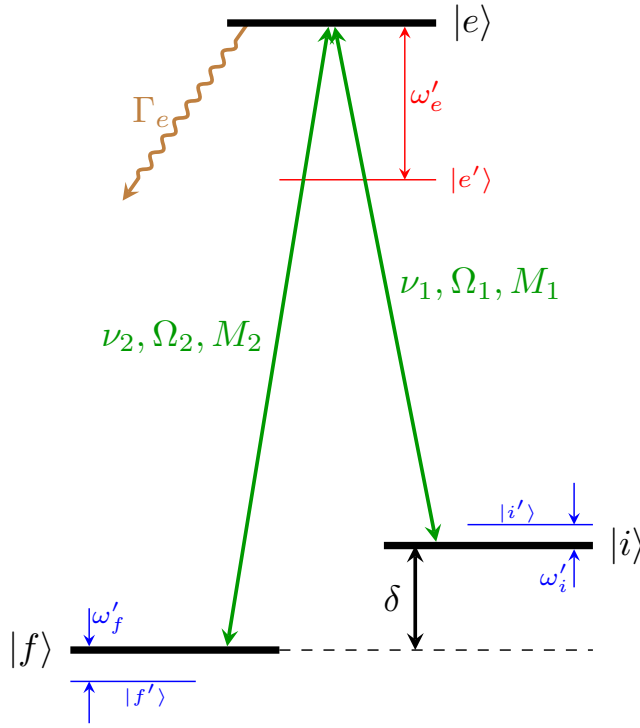
Figure 7.3: Generic model for a real STIRAP similar to Fig. 7.1. Differences are that the two beams are now on resonant with $|e\rangle$ and the Ω_1 and Ω_2 now represent the maximum single photon Rabi frequency during the STIRAP pulse.

is created due to a destructive interference of transition from the initial and final state to the excited state.

Similar to Raman transfer, STIRAP in an ideal three-level system can achieve full coherent transfer with arbitrarily small scattering probability when given unlimited time and power budget. However, in reality, states and coupling that exist outside the ideal three-level system always cause a non-zero probability of scattering loss (see Fig. 7.3). In this section, we will apply the approach we took for Raman transition to STIRAP. We will then compare the loss caused by different practical limitations and discuss which approach should be taken under certain circumstance.

7.3.1 Additional Initial and Final States

Similar to Raman transition (section 7.2.1), the additional initial and final states causes potential leakage out of the three-level system. This limits the minimum time of the transfer in a way similar to that of Raman transition.

7.3.2 Additional Excited states

7.3.3 Cross Coupling Between Light Addressing Initial and Final States

7.3.4 Conclusion

7.4 States Selection

(Differential Light Shift) (Scattering)

7.4.1 Excited State Selection

7.4.2 Ground States Selection

Final Molecular State

Initial Atomic State

7.5 Raman Transfer Results

7.5.1 Scaling of Raman Transition Parameters

8

Conclusion

A

Computer Control Hardware Specification

NI DAQ

FPGA

DDS

USRP

B

Full Raman Sideband Cooling Sequence

Each Raman pulse in the cooling sequence is followed immediately by an optical pumping pulse. The full parameters for the Raman pulses, including the cooling "axis", the sideband "order (Δn)", the cooling frequency "δ'", the carrier $(\Delta n = 0)$ frequency "δ'_0", the pulse "duration", the pulse strength in "Ω_0", and the beam of which a non-uniform "power ramp" is applied, are listed in 6 groups below. The applied cooling frequency, δ', is the two-photon detuning given relative to the

zero-field $F = 1$ and $F = 2$ hyperfine splitting of $1.7716261288(10)\,\text{GHz}$[Steck]. Due to the Stark shifts of the Raman beams, the carrier transition, $\delta_0^\vee$, varies with the power of the Raman beams. $\delta_0^\vee$ is given also relative to the zero-field hyperfine splitting. The strength of the pulses given in Ω_0 determines the two-photon Rabi frequency, $\Omega_{n,\Delta n} = \Omega_0 \langle n | e^{i\vec{k}\cdot\vec{r}} | n + \Delta n \rangle$. We adopt the convention that a π-pulse between state n and $n + \Delta n$ requires a duration $\pi/\Omega_{n,\Delta n}$. The difference between $\delta^\vee$ and $\delta_0^\vee$ gives the motional sideband frequency, δ. Many Raman pulses include a "power ramp" with a Blackman envelope[Kasevich & Chu] to minimize off-resonant excitations. Because each Raman pulse is a product of two spatial- and temporal-overlapped laser beams, the "power ramp" is applied only to the beam that has the smaller light shift (we label the beam by the corresponding F number) while the other beam has a square-pulse shape. For a Raman pulse with a power ramp, the Rabi frequency gives the arithmetic mean over the duration of the pulse.

Group 1

This group is repeated 4 times.

Axis	Δn	δ' (MHz)	δ'_0 (MHz)	Duration (μs)	Ω_0 (kHz)	Power ramp
x	-2	19.625	18.649	44.1	$2\pi \times 23$	F1
y	-2	19.615	18.648	28.6	$2\pi \times 35$	F1
x	-1	19.130	18.649	36.9	$2\pi \times 23$	F1
y	-1	19.615	18.648	24.0	$2\pi \times 35$	F1

Group 2

This group is repeated 5 times.

Axis	Δn	δ' (MHz)	δ'_0 (MHz)	Duration (μs)	Ω_0 (kHz)	Power ramp
z	-5	19.030	18.605	81.5	$2\pi \times 16$	F2
x	-2	19.625	18.649	44.1	$2\pi \times 23$	F1
z	-4	18.940	18.605	76.3	$2\pi \times 16$	F2
y	-2	19.615	18.648	28.6	$2\pi \times 35$	F1
z	-5	19.030	18.605	81.5	$2\pi \times 16$	F2
x	-1	19.130	18.649	36.9	$2\pi \times 23$	F1
z	-4	18.940	18.605	76.3	$2\pi \times 16$	F2
y	-1	19.130	18.648	24.0	$2\pi \times 35$	F1

Group 3

This group is repeated 6 times.

Axis	Δn	δ' (MHz)	δ'_0 (MHz)	Duration (μs)	Ω_0 (kHz)	Power ramp
z	-4	18.940	18.605	76.3	$2\pi \times 16$	F2
x	-2	19.625	18.649	44.1	$2\pi \times 23$	F1
z	-3	18.858	18.605	70.2	$2\pi \times 16$	F2
y	-2	19.615	18.648	28.6	$2\pi \times 35$	F1
z	-4	18.940	18.605	76.3	$2\pi \times 16$	F2
x	-1	19.130	18.649	36.9	$2\pi \times 23$	F1
z	-3	18.858	18.605	70.2	$2\pi \times 16$	F2
y	-1	19.130	18.648	24.0	$2\pi \times 35$	F1

Group 4

This group is repeated 7 times.

Axis	Δn	δ' (MHz)	δ'_0 (MHz)	Duration (μs)	Ω_0 (kHz)	Power ramp
z	-3	18.858	18.605	70.2	$2\pi \times 16$	F2
x	-2	19.625	18.649	44.1	$2\pi \times 23$	F1
z	-2	18.773	18.605	62.7	$2\pi \times 16$	F2
y	-2	19.615	18.648	28.6	$2\pi \times 35$	F1
z	-3	18.858	18.605	70.2	$2\pi \times 16$	F2
x	-1	19.130	18.649	36.9	$2\pi \times 23$	F1
z	-2	18.773	18.605	62.7	$2\pi \times 16$	F2
y	-1	19.130	18.648	24.0	$2\pi \times 35$	F1

GROUP 5

This group is repeated 10 times.

Axis	Δn	δ' (MHz)	δ'_0 (MHz)	Duration (μs)	Ω_0 (kHz)	Power ramp
z	-2	18.773	18.605	62.7	$2\pi \times 16$	F2
x	-1	19.130	18.649	36.9	$2\pi \times 23$	F1
z	-1	18.685	18.605	52.5	$2\pi \times 16$	F2
y	-1	19.130	18.648	24.0	$2\pi \times 35$	F1
z	-2	18.773	18.605	62.7	$2\pi \times 16$	F2
x	-1	19.130	18.649	70.0	$2\pi \times 23$	F1
z	-1	18.685	18.605	52.5	$2\pi \times 16$	F2
y	-1	19.130	18.648	46.0	$2\pi \times 35$	F1

Group 6

This group is repeated 30 times.

Axis	Δn	δ' (MHz)	δ_0' (MHz)	Duration (μs)	Ω_0 (kHz)	Power ramp
z	-1	18.683	18.605	78.7	$2\pi \times 11$	F2
z	-1	18.683	18.605	135.0	$2\pi \times 11$	F2
z	-1	18.685	18.605	78.7	$2\pi \times 11$	F2
x	-1	19.130	18.649	36.9	$2\pi \times 23$	F1
y	-1	19.130	18.648	24.0	$2\pi \times 35$	F1
z	-1	18.685	18.605	78.7	$2\pi \times 11$	F2
z	-1	18.685	18.605	135.0	$2\pi \times 11$	F2
z	-1	18.685	18.605	78.7	$2\pi \times 11$	F2
x	-1	19.130	18.649	70.0	$2\pi \times 23$	F1
y	-1	19.130	18.648	46.0	$2\pi \times 35$	F1

References

[Hutzler et al.] Hutzler, N. R., Liu, L. R., Yu, Y., & Ni, K.-K. Eliminating light shifts for single atom trapping. 19(2), 023007.

[Kasevich & Chu] Kasevich, M. & Chu, S. Laser cooling below a photon recoil with three-level atoms. 69(12), 1741–1744.

[Kaufman et al.] Kaufman, A. M., Lester, B. J., & Regal, C. A. Cooling a Single Atom in an Optical Tweezer to Its Quantum Ground State. 2(4), 041014.

[Meekhof et al.] Meekhof, D. M., Monroe, C., King, B. E., Itano, W. M., & Wineland, D. J. Generation of Nonclassical Motional States of a Trapped Atom. 76(11), 1796–1799.

[Steck] Steck, D. A. Sodium D Line Data.

[Thompson et al.] Thompson, J. D., Tiecke, T. G., Zibrov, A. S., Vuletić, V., & Lukin, M. D. Coherence and Raman Sideband Cooling of a Single Atom in an Optical Tweezer. 110(13), 133001.